Journal of Electroanalytical Chemistry 635 (2009) 7–12

Contents lists available at ScienceDirect

Journal of Electroanalytical Chemistry

journal homepage: www.elsevier.com/locate/jelechem

Electrogenerated chemiluminescence (ECL) of 2-oxa-bicyclo[3.3.0]octa-4,8-diene-3,6-dione (**OBDD**)

Anahita Izadyar [a], Shiuh-Tzung Liu [b], Pi-Tai Chou [b], Allen J. Bard [a,*]

[a] Center for Electrochemistry, The University of Texas at Austin, Chemistry and Biochemistry Department, Austin, TX 78712, USA
[b] Department of Chemistry and Instrumentation Center, National Taiwan University, Taipei 106, Taiwan

ARTICLE INFO

Article history:
Received 20 March 2009
Received in revised form 8 July 2009
Accepted 27 July 2009
Available online 6 August 2009

Keyword:
Electrogenerated chemiluminescence

ABSTRACT

We report the electrogenerated chemiluminescence (ECL) of 2-oxa-bicyclo[3.3.0]octa-4,8-diene-3,6-dione (**OBDD**). Cyclic voltammetry at 100 mV/s shows two chemically reversible reduction waves but an irreversible oxidation wave. As opposed to the usual radical ion annihilation ECL, for this compound, ECL was observed in an acetonitrile solution just upon oxidation to the radical cation (D^+) in the absence of any additional coreactant. This suggests that **OBDD** can produce the needed reducing species upon its oxidation, so ECL is probably generated by the reaction of D^+ with a strongly-reducing free radical produced during **OBDD** electrooxidation. Production of CO_2 upon oxidation was found by bulk electrolysis and mass spectrometry.

1. Introduction

We describe the electrochemistry and electrogenerated chemiluminescence (ECL) processes of an interesting new laser dye, 2-oxa-bicyclo[3.3.0]octa-4, 8-diene-3, 6-dione (**OBDD**) with a high fluorescence quantum yield (~1) [1], that behaves as the emitting species and also generates, in a coreactant-like way, the needed strong reductant to produce the excited state.

ECL has been extensively investigated and has found many applications [2–6]. The simplest ECL process is the radical ion annihilation reaction sequence represented as:

$$R - e^- \rightarrow R^{+\cdot} \quad \text{(oxidation at electrode)} \tag{1}$$

$$R + e^- \rightarrow R^{-\cdot} \quad \text{(reduction at electrode)} \tag{2}$$

$$R^{+\cdot} + R^{-\cdot} \rightarrow {}^1R^* + R \quad \text{(singlet excited state formation)} \tag{3}$$

$$ {}^1R^* \rightarrow R + h\nu \quad \text{(light emission)} \tag{4}$$

Many ECL reactions of this type have been investigated and their mechanisms are well understood. These reactions generally involve the use of anhydrous and deoxygenated nonaqueous solvents to accommodate the large potential range required to generate these energetic precursors, R and R^+, to produce an excited state in the visible region (1.8–3.0 eV) [7].

ECL can also be generated through the use of coreactants, whose electrochemical reaction can generate energetic oxidants or reductants by bond cleavage, which can then particpate in the redox reaction with the radical ion. Typical coreactants are $C_2O_4^{2-}$ (generating $CO_2^{\cdot-}$ on oxidation) and $S_2O_8^{2-}$ (generating $SO_4^{\cdot-}$ on reduction). These allow generation of ECL on a single pulse in one direction, e.g. to positive potentials. In this case the reductants must be energetic enough to react with the radical cations of the emitter to produce their excited states. Typical coreactants for oxidations are tri-*n*-propylamine (TPrA), which produces a strong reducing agent (TPrA) [8], and oxalate ion ($C_2O_4^{2-}$), which upon oxidation, loses CO_2, producing $CO_2^{\cdot-}$, a strong reducing agent [9–12]. The ECL mechanism based on a radical cation and oxalate is as follows [4]:

$$R^{+\cdot} + C_2O_4^{2-} \rightarrow R + C_2O_4^{\cdot-} \tag{5}$$

$$C_2O_4^{\cdot-} \rightarrow CO_2^{\cdot-} + CO_2 \tag{6}$$

$$R^{+\cdot} + CO_2^{\cdot-} \rightarrow R^* + CO_2 \tag{7}$$

$$R + CO_2^{\cdot-} \rightarrow R^{-\cdot} + CO_2 \tag{8}$$

followed by reaction (4).

Alternatively, a coreactant can be used in a reducing step by an analogous route. For example, peroxydisulfate ($S_2O_8^{2-}$) [13,14] and benzoylperoxide (BPO) [15,16] produce strong oxidizing agents on reduction.

Electrochemical and spectroscopic measurements of **OBDD** were performed. **OBDD** is a highly fluorescent molecule that exhibits unity fluorescence quantum yield and a short radiative lifetime (<4 ns) in common organic solvents. The π–π^* transition character has been fully justified via theoretical approaches. This compound also demonstrates remarkable amplified spontaneous emission with a gain efficiency of >10 and with excellent photostability, making **OBDD** a potentially novel laser dye that incorporates a bicyclic, fused five-membered lactones ring structure. Future application of this dye is wide ranging. For example, through

* Corresponding author. Tel.: +1 512 471 3761; fax: +1 512 471 0088.
E-mail address: ajbard@mail.utexas.edu (A.J. Bard).

0022-0728/$ - see front matter © 2009 Elsevier B.V. All rights reserved.
doi:10.1016/j.jelechem.2009.07.020

strategic design of the substituent on the phenyl group, syntheses of water-soluble fluorescent dyes can be achieved, such that their applications toward fluorescent imaging and biomolecular recognition become feasible [1].

In this paper, we show that **OBDD** emits light when oxidized in the absence of coreactant, presumably because carbon dioxide is produced during the oxidation of **OBDD**, and the radical anion of CO_2 could act as an internal coreactant. This phenomenon is uncommon in the literature, but has been observed for tranquilizer chlorpromazine (CPZ) [17–20].

2. Experimental

2.1. Chemicals

The 2-oxa-bicyclo[3.3.0]octa-4,8-diene-3,6-dione (**OBDD**) was synthesized as previously described [1]. Anhydrous acetonitrile (MeCN, 99.8% in a sure-sealed bottle) was obtained from Aldrich. Tetra-*n*-butylammonium perchlorate (TBAP) was obtained from Fluka and transferred directly into the drybox. All solutions were prepared in the drybox in an airtight cell for measurements outside the drybox.

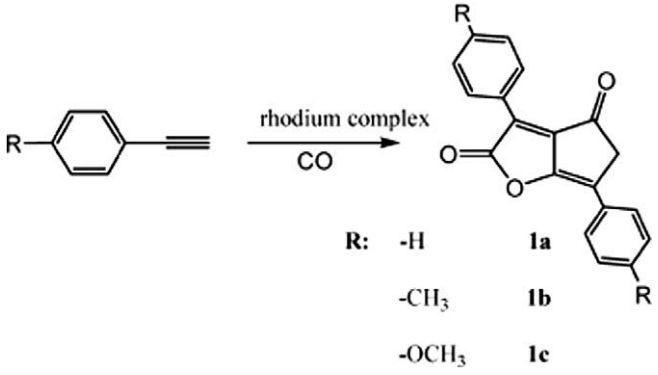

Fig. 1. Molecular structure of 2-oxa-bicyclo[3.3.0]octa-4,8-diene-3,6-dione **OBDD**) (compound 1a) and related species.

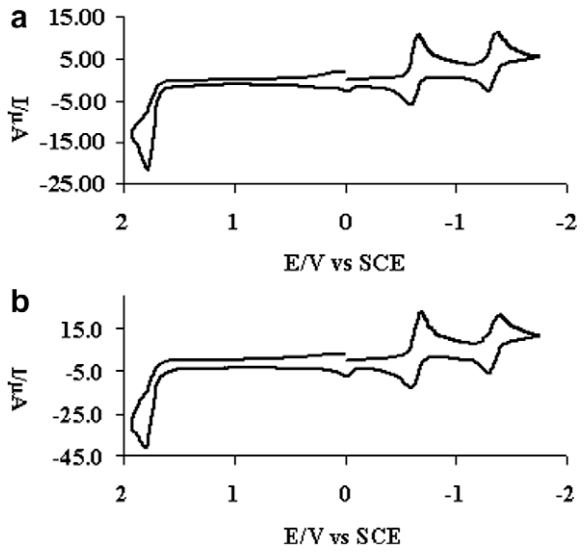

Fig. 2. Cyclic voltammograms of 1 mM **OBDD** in acetonitrile with 0.1 M TBAP as the supporting electrolyte. Working electrode is a Pt disk with diameter 0.5 mm. Scan rates were (a) 0.1 V/s and (b) 20 V/s.

2.2. Apparatus and instrumentation

All fluorescence spectra were recorded on a Fluorolog-3 spectrofluorimeter (ISA-Jobin Yvon Horiba, Edison, NJ), using a slit width of 0.5 mm. UV–vis spectra were recorded on a Milton Roy Spectronic 3000 array spectrophotometer.

Cyclic voltammograms (CVs) were recorded on a CH Instruments electrochemical work station Model 660 (Austin, TX). The working electrode, in most cases, consisted of an inlaid Pt disk (1–2 mm in diameter) that was polished on a felt pad with 0.3 μm, followed by 0.05 μm, alumina (Buehler, Ltd., Lake Bluff, IL), sonicated in water and absolute ethanol for 5 min, and dried in an oven at 100 °C before being transferred into the inert atmosphere drybox. A J-shaped electrode was used for ECL intensity measurements. A Pt wire served as a counter electrode and a Ag wire as a quasi-reference electrode (QRE). The ECL spectra were taken using a charge coupled device (CCD) camera (Princeton Instruments, SPEC-10) that was cooled to −100 °C. The CCD camera and holographic spectrometer were calibrated with a mercury lamp. ECL intensity–time curves were monitored with a photomultiplier tube (PMT, Hammatsu, R4220p) equipped with an electrometer (Keithley 6517). The output of the electrometer was acquired with the ADC module of an Auto lab potentiostat (Ecochemie). The PMT was supplied with 750 V from a high voltage power supply (Series 225, Bertan High Voltage Corp, Hucksville, NY). All potentials were calibrated against SCE by the addition of ferrocene (Fc) as an internal standard, taking $E^{o}_{Fc/Fc+} = 0.424$ V, vs. SCE. Mass spectroscopy results were measured on LCQ (Thermo) and liquid chromatography were measured on Magic 2002 (Michrom BioResources, Inc.).

All ECL measurements were performed as previously reported [21]. To generate ECL via an ion annihilation reaction, the working electrode was pulsed between the first oxidation and reduction peak potentials with a pulse width of 0.1 s.

Digital simulations of cyclic voltammograms were performed with the Digisim Software package (BAS, West Lafayette, IN) to investigate the mechanisms of the electrochemical processes, taking into account the uncompensated resistance (~500 Ω). Molecular modeling was carried out with Hyperchem.

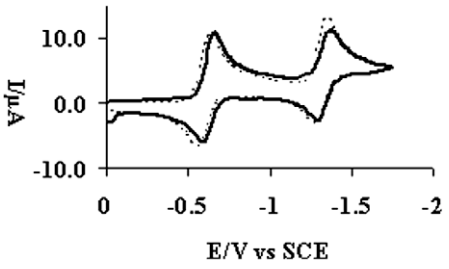

Fig. 3. Experimental (solid line) and simulated (dotted line) cyclic voltammograms for the reduction peaks (scan rate 0.1 V/s, 1 mM).

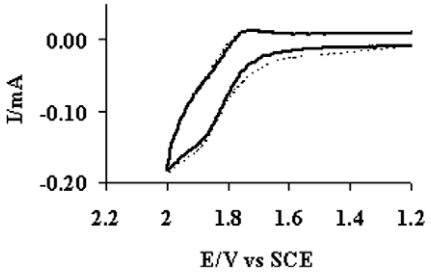

Fig. 4. Experimental (solid line) and simulated (dotted line) cyclic voltammograms for the oxidation peak (scan rate 20 V/s, 1 mM).

A three-electrode configuration was used, with a large platinum screen as working electrode, a platinum screen electrode as counter electrode and a silver wire coated with partially oxidized polypyrrole as a QRE for bulk electrolysis [22]. The silver quasi-reference electrode (AgQRE) was separated from the working electrode by a capillary tube in the first compartment of the cell. The second compartment contained only supporting electrolyte solution, and the third one contained the counter electrode in the supporting electrolyte solution. The compartments were separated by fine porosity frits. We carried out the bulk electrolysis of the solution by applying 1.7 V vs. SCE for 30 min at the working electrode under convection with a magnetic stirrer.

3. Results and discussion

3.1. Electrochemistry

The electrochemical behavior of **OBDD** (Fig. 1) was investigated to find the potentials for reduction and oxidation and to determine the stability of the electrogenerated products. The cyclic voltammograms obtained consist of two reversible reduction waves at peak potentials of 0.70 and 1.40 V vs. SCE. These chemically reversible reductions correspond to the formation of the radical anion and dianion (Fig. 2). These waves show i_{pa} and i_{pc} proportional to $v^{1/2}$ and near equality of the peak currents indicating diffusion control and slow following chemical reactions. At low scan rates, both reduction peaks are essentially nernstian, one-electron processes, as judged from the peak separation (taking into consideration uncompensated resistance, $R_u \sim 500\,\Omega$ ($\Delta E_p = 63$ mV). A small anodic peak near 0 V was seen only upon traversing the second reduction peak, suggesting some contribution of a following reaction of the dianion (probably protonation).

Cyclic voltammograms (CVs) at different scan rates are shown in Fig. 2 (and Figure S1 in the Supporting Information). The diffusion coefficient was determined from the first reduction wave using the Randles–Sevick equation [23] for several scan rates. For this compound, the diffusion coefficient (D) was about 1.3×10^{-5} cm^2/s and adjusted to fit the data [24].

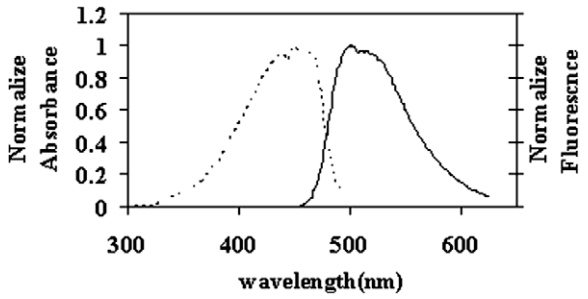

Fig. 5. Absorbance and fluorescence of **OBDD** (4 μM) in acetonitrile.

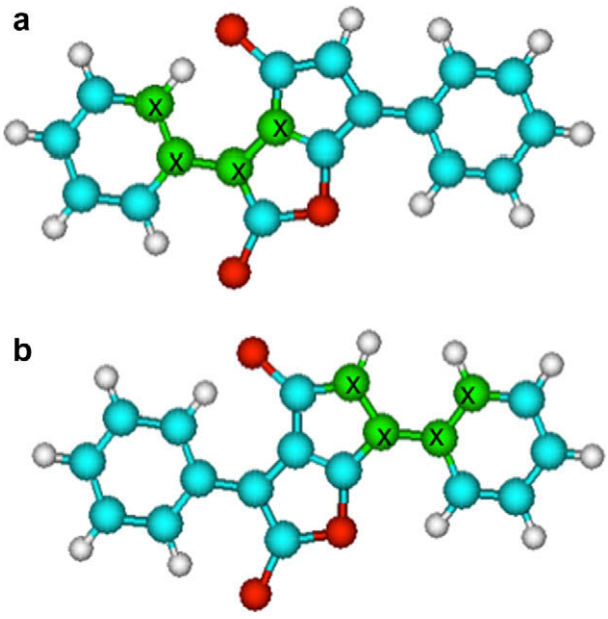

Fig. 6. The **OBDD** molecular model (a) torsion angle of atoms 4–6–7–8 is 0°, (b) torsion angle of atoms 15–13–19–17 is ~0° (atoms have an 'x').

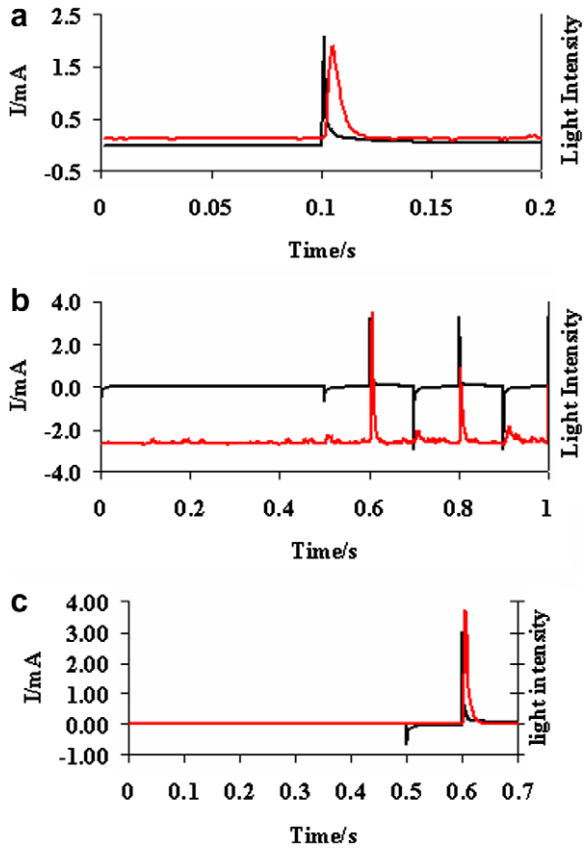

Fig. 7. (a) Intensity–time curve for **OBDD** ECL, generated by 0.1 s pulse between 0.0 V and +1.90 V vs. Ag wire QRE. (b) Intensity–time curve for **OBDD** ECL, generated by 0.1 s pulses by alternating potential between −0.80 V and +1.90 V vs. Ag wire QRE (0.7 s pulse time duration). (c) Intensity–time curve for **OBDD** ECL, generated by 0.1 s pulses by alternating potential between −0.80 V and +1.90 V vs. Ag wire QRE (1.0 s pulse time duration).

Table 1
Electrochemical data for **OBDD**.

E^{red}_{pc1} (V vs. SCE)[a]	E^{red}_{pc2} (V vs. SCE)[a]	E^{ox}_{pa} (V vs. SCE)[b]	$-\Delta G_{ann}$(app) (eV)[c]	$-\Delta H_{ann}$(app) (eV)[d]	E_s (eV)[e]
−0.70	−1.40	+1.70	2.40	2.30	2.41

[a] Reduction, cathodic peak potentials of 2-oxa-bicyclo[3.3.0]octa-4,8-diene-3,6-dione V vs. SCE.
[b] Oxidation, anodic peak potentials of compound in MeCN; 0.1 M TBAP.
[c] $-\Delta G_{ann} = E^{OX}_{pa} - E^{red}_{pc}$.
[d] $-\Delta H_{ann} = -\Delta G_{ann} - 0.1$.
[e] $E_s = 1239.85/\lambda^{PL}_{max}$ (nm).

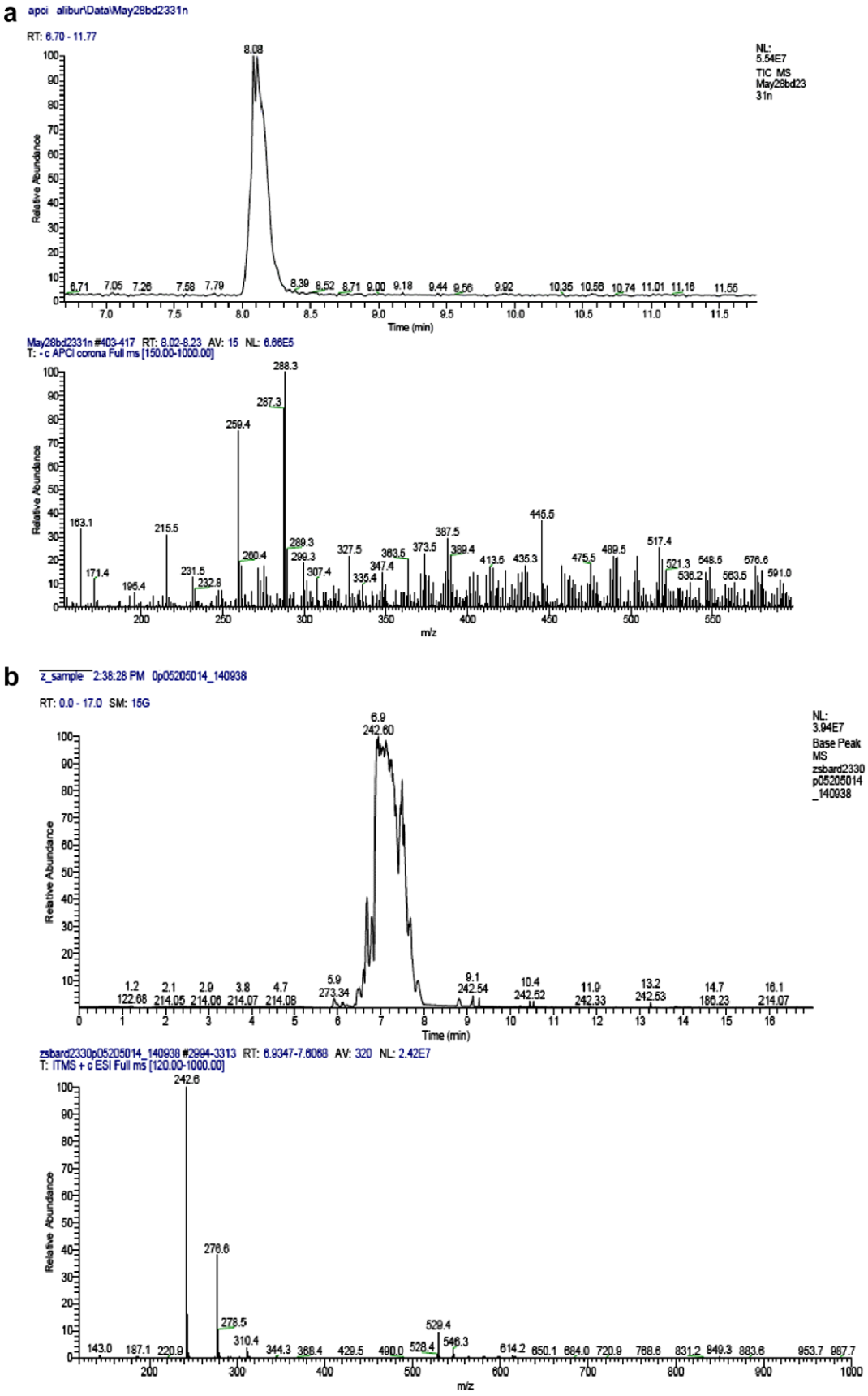

Fig. 8. (a) The mass spectrum of **OBDD** before bulk oxidation. The spectrum displays a strong molecular ion at m/e = 288. (b) The mass spectrum of **OBDD** after bulk oxidation. The spectrum displays a strong molecular ion at m/e = 242.6. The base peak in spectrum below shows loss of a CO_2 after electrolysis.

The mechanism for the reductions can be modeled with DigiSim as a quasireversible first electron transfer.

$$A + e \leftrightarrows B \qquad k^\circ = 0.006\ \text{cm/s},\ E^\circ = -0.66\ \text{V vs. SCE} \tag{9}$$

and an EC second electron transfer (Fig. 3, and Figure S2 in the Supporting Information).

$$B + e \leftrightarrows C \qquad k^\circ = 0.002\ \text{cm/s},\ E^\circ = -1.4\ \text{V vs. SCE} \tag{10}$$

$$C \leftrightarrows D \qquad K_{eq} = 0.13, k_f = 0.1\ \text{s}^{-1} \tag{11}$$

The heterogeneous electron transfer rate constants k° found by the simulation seem unreasonably small, perhaps because of incomplete consideration of uncompensated resistance.

During the anodic scan, at low scan rates, e.g. 100 mV/s, an irreversible oxidation peak was observed with a peak current somewhat higher than that for the reduction, probably because of a contribution of background current at this rather positive potential. At a higher scan rate, e.g. 20 V/s, some reversibility of the oxidation was seen. Simulations of CVs for the oxidation waves were carried out for different scan rates for an EC_r scheme (Fig. 4, and Figure S3 in the Supporting Information).

$$A - e \leftrightarrows B \qquad k^\circ = 0.106\ \text{cm/s}, E^\circ = 1.8\ \text{Vvs. SCE} \tag{12}$$

$$B \leftrightarrows C \qquad K_{eq} = 3.28 \times 10^6, k_f = 555.11\ \text{s}^{-1} \tag{13}$$

In the simulations, α was taken to be 0.5. Diffusion coefficient was assigned to be $1.3 \times 10^{-5}\ \text{cm}^2/\text{s}$.

3.2. Spectroscopy

Molecular absorption spectroscopy of **OBDD** was investigated over a range of concentrations (1.6×10^{-7}–4.0×10^{-6} M). The extinction coefficient, at the $S_0 \rightarrow S_1$ absorption band maximum, 441 nm, was $\varepsilon = 3.8 \times 10^4\ \text{M}^{-1}\ \text{cm}^{-1}$. Absorption and fluorescence spectra of **OBDD** at a concentration of 4 μM in acetonitrile are shown in Fig. 5. Fluorescence was observed in the blue–green[1] region ($\lambda_{max} = 514$). A stokes shift of $\Delta\lambda = 73$ nm was observed. The small shift was attributed to the minimal reorganization in the excited state, consistent with a ground state rigid and planar structure, as calculated by molecular modeling (MNDO) and shown in Fig. 6.

3.3. Electrogenerated chemiluminescence

By alternately pulsing the electrode potential between the first reduction peak potential of **OBDD**, 0.7 V vs. SCE, and the oxidation peak potential,+1.7 V, with a pulse width 0.1 s and recording the total emission with a PMT, we were able to detect ECL (Fig. 7, and Figures S4 and S5 in the Supporting Information). However, the instability of the radical cation caused rapid decay of the light intensity with time, and we were unable to sustain the ECL long enough to obtain an ECL spectrum.

Because of the cation radical instability, less would be available to produce ECL during the cathodic pulse and one would expect the ECL signal to be more intense during the anodic step. However, as shown in Fig. 7a and b (and Figure S6 in the Supporting Information), the ECL signal was more intense for the cathodic pulses (Fig. 7b). A summary of the electrochemical and spectroscopic data relevant to the energetics of annihilation ECL is shown in Table 1. The apparent free energy and enthalpy of the radical anion annihilation, ΔG_{ann}(app) and ΔH_{ann}(app), appear marginal or too small to directly populate the singlet state. However, the actual E^o for radical cation formation is more positive than that given by the E_{pa}, because the following decomposition reaction causes the peak to shift to less positive potentials. Thus the annihilation probably proceeds by direct population of the singlet, with the low intensity attributed to reactant instability.

Surprisingly, emission of light was also observed during the first anodic pulse, when no radical anion was present in the working electrode diffusion layer. To make sure the light recorded on the PMT was only from the working electrode, we blocked any possible light emission from the counter electrode by masking the cell with black electrical tape placed on the outside of the glass optical window. Since no coreactant was purposely added, this ECL presumably follows an "internal coreactant" mechanism or is caused by an adventitious impurity acting as a coreactant on oxidation.

The unusual observation of ECL simply by an oxidation process suggests that during the oxidation the product undergoes a decomposition reaction to produce a strong reductant that reacts with the unstable radical cation to produce an excited state. A familiar intermediate is $CO_2^{\cdot-}$, which is a strong reductant; this route involves the loss of CO_2 from **OBDD**, but the mechanism is unknown. It would have to involve electron transfer followed by proton loss. We attempted to analyze the products after bulk electrolysis in a three-compartment cell under oxidizing conditions. The investigation of CVs before and after following bulk oxidation at 1.7 V (scan rate = 100 mV/s) demonstrated only partial disappearance of the parent species. The products were analyzed by photoluminescence and also by mass spectroscopy (HPLC–ESI-MS). Although the electrolysis was not complete, the mass spectroscopy of samples before and after bulk oxidation suggested that **OBDD** lost CO_2 from electrolytic oxidation. The molecular ion is seen at m/z = 288. Fragmentation via loss of 44 ($-CO_2$) gives a common fragment at m/z = 244 (Fig. 8a andb). Fig. 8b shows the mass spectrum of **OBDD** after bulk oxidation. The spectrum displays a strong molecular ion at m/e = 242.6 which suggests loss of CO_2 during electrolysis. However a more detailed study will be required to discover the overall reaction path.

4. Conclusions

The ECL properties of 2-oxa-bicyclo[3.3.0]octa-4, 8-diene-3, 6-dione (**OBDD**) was investigated. We report the self-coreactant mechanism for **OBDD**, by producing the intermediate reducing agent CO_2 during the electrooxidation of **OBDD**. Intense, but unstable, ECL emission was observed when the potential is pulsed between zero and the oxidation potential. The products of exhaustive oxidation were analyzed by mass spectroscopy (HPLC–ESI-MS) which suggests loss of CO_2 during electrolysis.

Acknowledgments

The support by the National Science Foundation (CHE-0451494) and the Robert A. Welch Foundation (F-0021) is gratefully acknowledged. We also appreciate helpful discussions with Dr. Fu-Ren (Frank) Fan, Dr. Matthew Sartin and Khalid Omar throughout this work.

Appendix A. Supplementary data

Supplementary data associated with this article can be found, in the online version, at doi:10.1016/j.jelechem.2009.07.020.

References

[1] C.-Y. Wang, Y.-S. Yeh, E.Y. Li, Y.-H. Liu, S.-M. Peng, S.-T. Liu, P.-T. Chou, Chem. Commun. (2006) 2693.
[2] A.J. Bard, Electrogenerated Chemiluminescence, Marcel Dekker, NY, 2004. pp. 736–745.
[3] L.R. Faulkner, A.J. Bard, Electroanalytical Chemistry, vol. 10, Marcel Dekker, New York, 1977. p. 1.

[1] For interpretation of color in Fig. 6, the reader is referred to the web version of this article.

[4] A.W. Knight, G.M. Greenway, Analyst 119 (1994) 879.
[5] A.J. Bard, J.D. Debad, J.K. Leland, G.B. Sigal, J.L. Wilbur, J.N. Wohlsatdter, in: R.A. Meyers (Ed.), Chemiluminescence, vol. 11, Wiley, NY, 2000, pp. 9842–9849.
[6] M.A. Richter, Chem. Rev. 104 (2004) 3003.
[7] R.Y. Lai, A.J. Bard, J. Phys. Chem. A 107 (2003) 3335–3340.
[8] J.B. Noffsinger, N.D. Danielson, Anal. Chem. 59 (1987) 865.
[9] W. Miao, J.P. Choi, A.J. Bard, J. Am. Chem. Soc. 124 (2002) 14478.
[10] Y. Zu, A.J. Bard, Anal. Chem. 72 (2000) 223.
[11] Y. Zu, A.J. Bard, Anal. Chem. 73 (2001) 3960.
[12] M.M. Chang, T. Saji, A.J. Bard, J. Am. Chem. Soc. 99 (1977) 5399.
[13] A.G. Hadd, J.W. Briks, in: R.E. Sievers (Ed.), Peroxyoxalate Chemiluminescence, Wiley, NY, 1995.
[14] F. Bolletta, M. Ciano, V. Balzani, N. Serpone, Inorg. Chim. Acta 62 (1982) 207–213.
[15] H.S. White, A.J. Bard, J. Am. Chem. Soc. 104 (1982) 6891.
[16] J.-P. Choi, K.-T. Wong, Y.-M. Chen, J.-K. Yu, P.-T. Chou, A.J. Bard, J. Phys. Chem. B 107 (2003) 14407.
[17] T.C. Richards, A.J. Bard, Anal. Chem. 67 (1995) 3140–3147.
[18] J.A. Holeman, N.D. Danielson, Anal. Chim. Acta 277 (1993) 55.
[19] G.J. Siegel, R.W. Albers, R. Katzman, B.W. Agranoff, Basic Neurochemistry, third ed., Little Brown and Co., Boston, 1981.
[20] H.Y. Cheng, P.H. Sackett, R.L. McCreery, J. Am. Chem. Soc. 100 (1978) 962.
[21] P. McCord, A.J. Bard, J. Electroanal. Chem. 318 (1991) 91.
[22] J. Ghilane, P. Hapiot, A.J. Bard, Anal. Chem. 78 (2006) 6868–6872.
[23] A.J. Bard, L.R. Faulkner, Electrochemical Methods, second ed., Wiley, NY, 2000. p. 231.
[24] K. Kadish, J. Ding, T. Malinski, Anal. Chem. 56 (1984) 1741.